Stress Analyses of Mechanically Fastened Joints in Aircraft Fuselages

J.J.M. de Rijck[1], S.A. Fawaz [2], J. Schijve[3], R. Benedictus[3] and J.J. Homan[3]

[1] Corus RD&T, PO BOX 1000, 1970 CA IJmuiden, The Netherlands, Reinier.de-rijck@Corusgroup.com
[2] USAF Acadamy, 2354 Fairchild Drive, Suite 6L-155, USAF Acadamy, CO 80840, Scott.Fawaz@usafa.af.mil
[3] Delft University of Technology, Kluyverweg 1, 2629 HS Delft, The Netherlands, J.Schijve@lr.tudelft.nl, R.Benedictus@lr.tudelft.nl, J.J.Homan@lr.tudelft.nl

Abstract: For mechanically fastened lap-splice joints and butt joints in a fuselage structure the dominant loading condition is introduced by the ground-air-ground pressurization cycle. The hoop load is transferred from one skin panel to the next panel by fasteners in a lap joint or a single strap butt joint. The hoop load is offset by eccentricities in the joint, resulting in secondary bending. Secondary bending is highly dependent on the magnitude of the eccentricity and the flexural rigidity of the joint between the fastener rows. The bending stresses can be derived with a one-dimensional Neutral Line Model (NLM) as proposed by Schijve. In the present paper this model is extended to account for load transmission by rivet rows between the outer rows of the joint which was ignored in the original model. Strain gage measurements have indicated that load transmission occurs in these rows. The extended model covers both monolithic and fibre metal laminate materials. It can be applied to a wide range from simple to complicated joints containing rivets or bolt type fasteners. In case of riveted fasteners, the influence of so-called fastener flexibility can be addressed as well. Strain gage measurements on lab specimens and in-service joints have supported the analysis to show the most likely locations for fatigue crack nucleation and growth.

1. INTRODUCTION

A thorough understanding of the stresses at the most critical fastener row is essential in conducting fatigue and damage tolerance analysis of mechanically fastened joints. The critical fastener row location is most susceptible to fatigue crack nucleation and subsequent crack growth. The dominant loading condition for riveted lap-splice joints in an aircraft fuselage structure is introduced by the Ground-Air-Ground (GAG) pressurization cycle. The hoop load is transferred from one skin panel to the next panel by fasteners in a lap joint or a single strap

butt joint. The hoop load is not collinear through the joint because it is offset by eccentricities in the joint. The eccentric path of the hoop load causes secondary bending, see Figure 1 for a simple case. The total stress in the joint around the rivet holes is then the sum of the hoop stress, stresses due to secondary bending and bearing stress associated with the fastener loads on the holes. Load transmission by friction is not considered here. Secondary bending is highly dependent on the magnitude of the eccentricity and the flexural rigidity of the joint between the fastener rows. The theory used to derive the bending stresses is based on advanced beam theory [1]. Schijve adopted a simple Neutral Line Model (NLM) to calculate the tension and bending stresses at any location in the joint. It is important to know the secondary bending stress for indicating the most critical rivet row in a lap-splice joint [2], [3] in which the fatigue crack nucleation will occur. Well-known problems of multiple-site damage and damage tolerance are associated with crack nucleation at fastener holes.

The neutral line model is a one-dimensional model in such a way that the out of plane displacement of the neutral axis (*w(x)* in Figure 3) determines the behaviour of the joint as a single structural element. In the simple Neutral Line Model employed by Schijve load transmission occurs at the outer rivets only, and load transmission does not occur by fasteners in the middle row. The effect of local plastic deformation was considered by Schijve in a simple way by assuming that it caused a local rotation of the neutral line. A rotation of 1° caused already a significant reduction of the maximum bending moment in the joint, but load transmission by the middle rivet rows was still ignored.
Müller [4] considered load transfer by all rivet rows in an entirely different way. He introduced elastic fastener elements between the two sheets of a FE model. In this model the middle row is also transferring part of the load. The two outer rows were also the more critical rows in his model. The method proposed by Müller is not evaluated here because this method is based on changing the actual flexural rigidity to a virtual flexural rigidity. The method is adequate for joints made of monolithic materials, but does not allow for a correct calculation of the neutral line displacements for fiber metal laminates (FML) because both the elastic modulus and moment of inertia are changed.
In the present paper a new model is introduced based on the elastic Neutral Line Model. However, local plasticity around the rivet holes is assumed to occur. As a consequence, load transfer occurred at each rivet row, which results in different loads in the two mating sheets of the lap joint. The latter effect is dealt with by defining an internal moment. The load transmission is depending on the thicknesses of the sheets and the load on the joint. For illustrative purposes the original Neutral Line Model is discussed first in Section 2.1 for a simple symmetric lap joint. In Section 2.2 the new model is discussed for the same lap joint. A comparison is made between the bending stresses obtained with the simple Neutral Line Model and the present model.
The new model can also be applied to more complex splice joints of both monolithic and fiber metal laminates, e.g. GLARE. In the latter case the multilayer effect on the bending stiffness must be accounted for. Various results are presented in [6]. In Section 3 exemplary results are shown for the bending stress in a single strap butt joint of monolithic 2024-T3 and for a similar joint of Glare sheets. The results are compared to strain gage measurements. The paper is completed with some summarizing conclusions.

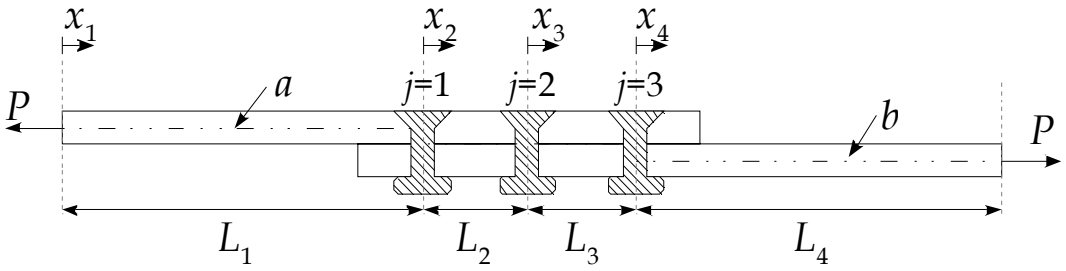

Figure 1 Nomenclature for lap-splice joint geometry

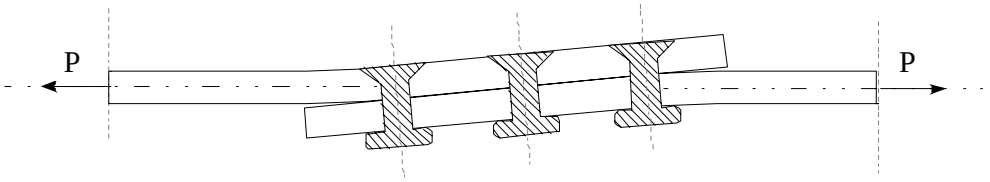

Figure 2 Tensile load P causes secondary bending of the lap-splice joint

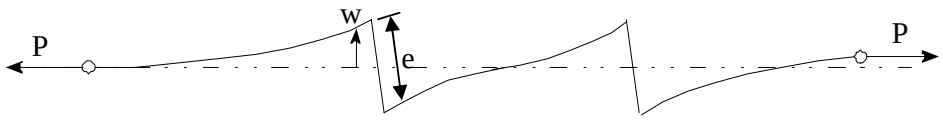

Figure 3 Neutral line model with out-of-plane displacement *w(x)*

2. THE NEUTRAL LINE MODEL FOR A SIMPLE LAP-JOINT MODEL

2.1 Original neutral line model

The origional neutral line model [3] for an simple lap-splice joint is recapitulated here in order to explain the extension of this model with fastener flexibility and the internal moment concept. The dimensions of the lap-splice joint with three rivet rows are shown in Figure 1. For simplicity symmetry is assumed which implies that $L_2 = L_3$ and $L_1 = L_4$. Both sheets are also similer $t_a = t_b$ and $E_1 = E_2$. If the specimen is loaded in pure tension then secondary bending will occur (Figure 2) and the neutral line becomes curved due to eccentricities inherent to lap-splice joints (Figure 3). In the original Neutral Line Model the two sheets between the outer fastener rows are assumed to behave as one integral sheet. It implies that load transfer does not occur in the middle row. Furthermore fastener flexibility is not considered.

With the notations of Figure 1 the bending moment can be written as:

$$M_x = Pw \tag{1}$$

For sheet bending:

$$M_x = EI\frac{d^2x}{dx^2} \tag{2}$$

The differential equation thus becomes:

$$\frac{d^2w}{dx^2} - \alpha^2 w = 0 \tag{3}$$

with

$$\alpha_i^2 = \frac{P}{EI_i} \quad (i=1,2) \tag{4}$$

The solution is:

$$w_i = A_i \sinh(\alpha_i x_i) + B_i \cosh(\alpha_i x_i) \tag{5}$$

A_i and B_i are solved using the boundary conditions for the two parts with length L_1 and L_2 respectively.

$$\begin{aligned} &x_1 = 0 \rightarrow w_1 = 0 \\ &x_1 = L_1 \; and \; x_2 = 0 \rightarrow w_2 = w_1 - e \\ &x_1 = L_1 \; and \; x_2 = 0 \rightarrow \frac{dw_1}{dx_1} = \frac{dw_2}{dx_2} \\ &x_2 = L_2 \rightarrow w_2 = 0 \quad (symmetry) \end{aligned} \tag{6}$$

After substitution of Eq. (5) in the in Eq. (6) the constants A_i and B_i of Eq. (5) can be solved. The bending moment M_x is then obtained as:

$$M_x = EI\left(\frac{d^2w}{dx^2}\right)$$

The maximum secondary bending occurs at the first fastener row ($x_1 = L_1$). Defining the bending factor k_b as:

$$k_b = \frac{\sigma_{bending}}{\sigma_{tension}} = \frac{\frac{6M_c}{Wt^2}}{\frac{P}{Wt}} = \frac{6\alpha_1^{\,2}A_1}{Pt} \tag{7}$$

the solutions derived in [3] for $t_a = t_b$ and $L_2 = L_3$ is:

$$k_b = \frac{3}{1 + 2\sqrt{2}\left(\frac{Th_2}{Th_1}\right)} \tag{8}$$

with the hyperbolic function $Th_i = \tanh(\alpha_i L_i)$ it was shown in [3] that for a long specimen, i.e. L_1 significantly larger then L_2, the value of Th_1 is practically equal to 1. This implies that the effect of the length of the specimen on the secondary bending can be ignored, and the equation reduces to:

$$k_b = \frac{3}{1 + 2\sqrt{2}\tanh(\alpha_2 L_2)} \tag{9}$$

with:

$$\alpha_2 = \sqrt{\frac{3\sigma}{2t^2 E}} \tag{10}$$

The loading conditions at the ends of the specimen, i.e. far away of the overlap region, were also explored in [3]. If the hinged load introduction in is replaced by a fixed clamping ($dw/dx_1 = 0$ at $x_1 = 0$) the difference of the secondary bending at $x_1 = L_1$ with the hinged load introduction is negligible. This also applies to a misalignment when the loads P at the two ends of the specimen are applied along slightly shifted parallel lines.

Values of the bending factor k_b calculated with (9) for different input data are shown in Table I. The data in the first line of the table applies to the geometry of typical specimen dimensions. The load P corresponds to an applied stress level of 100 MPa.

L_1 [mm]	L_2 [mm]	t [mm]	E [N/mm^2]	k_b for an applied stress of 100 MPa
200	28	2	72000	1.16
	18			1.43
	28	1		0.88
		2	210000	1.49

Table I Variation of input data for symmetrical lap-splice joint

The results in the table show the following trends:

- If the row spacing L_2 is reduced from 28 mm to 18 mm, the bending factor increases from 1.16 to 1.43
- If the sheet thickness is reduced from 2 mm to 1 mm, the bending factor decreases from 1.16 to 0.88
- If the Elasticity Modulus is increased from 72000 MPa (Al-alloys) to 210000 MPa (steel) the bending factor increases from 1.16 to 1.49

These trends can be understood as being related to the bending flexibility of the overlap region and the eccentricity in the joint. It may well be expected that similar trends will also

apply to lap-splice joints of fiber metal laminates, which also applies to the effects of specimen clamping (fixed or hinged and misalignment).

2.2 The model with the internal moment to account for load transmission

In the previous section load transfer from one sheet to the other sheet of a lap-splice joint occurred only by the fasteners in the 1st and 3rd row because fastener flexibility was ignored and the two sheets between the outer rivet rows were considered as a single beam with a thickness of $t_a + t_b$. However, due to the high stresses in the sheets around the fastener holes, some plastic deformation will occur around the holes. As a result some more rivet tilting will be possible. This will affect the load transfer and as a consequence load transfer will also occur by the middle row. An "internal moment" model is presented for solving this problem. As an illustration of the model, it is discussed here for the same symmetric lap splice joint discussed in the previous Section 2.1.

Because fastener flexibility is now considered load transmission from one sheet to the other sheet occurs by all three rows, also the middle row. The load transmitted by the three rows are T_1, T_2 and T_3 (see Figure 4), and because of the symmetry $T_3 = T_1$. Moreover, $P = T_1 + T_2 + T_3$ and thus:

$$P = 2T_1 + T_2 \tag{11}$$

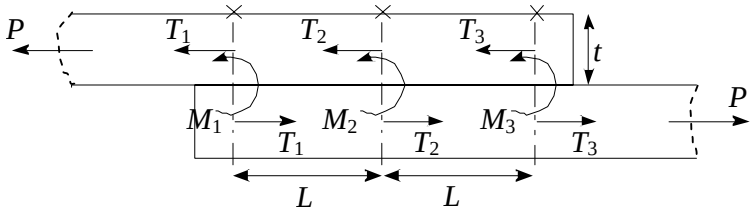

Figure 4 Simple lap-splice joint with load transmission from the upper sheet to the lower sheet causing internal moments

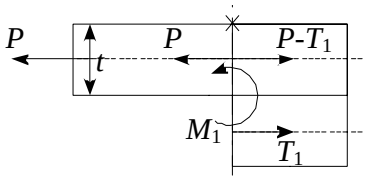

Figure 5 Internal moment as a result of load transfer via the fastener

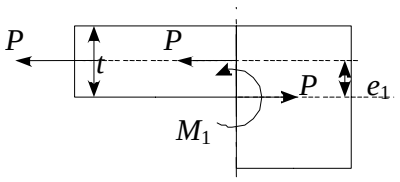

Figure 6 Moment as a result of the load transfer of original neutral line model

The loads in the various parts of the joint are indicated in Figure 4. In the elementary neutral line model, the middle row did not contribute to load transmission ($T_2 = 0$) and as a consequence T_1 and T_3 were both equal to $P/2$. However, due to fastener flexibility, T_1 and $P-T_1$ are no longer equal to $P/2$ because different tension loads occur in the upper and lower segments of the overlap of the joint. As a consequence, an internal moment will be introduced at the fastener rows, M_1, M_2 and M_3, at the three fastener rows respectively. In view of symmetry $M_3 = M_1$. The internal moment M_1 at the first fastener row is indicated in Figure 5. As mentioned earlier, the loads in the upper and lower sheet are different due to the load transfer associated with different tensile elongations of the upper and lower sheet. In the neutral line model the upper and lower sheets between the 1st and 3rd rivet row, in the overlap region, are assumed to act as an integral beam subjected to secondary bending.

$$\begin{aligned} &-M_1 + T_1\frac{t}{2} - T_1\frac{3}{2}t = 0 \\ &M_1 = -T_1 t \end{aligned} \tag{12}$$

This moment is associated with the influence of the load transfer of Figure 5 and thus the neutral line model will behave as shown in Figure 6. For the moment in the second and third fastener row using the same principle follows that:

$$\begin{aligned} M_2 &= -T_2 t \\ M_3 &= -T_1 t \end{aligned} \tag{13}$$

The original neutral line model calculates the (non-linear) secondary bending moment in a joint and assumes a moment introduced by the eccentricity e_1. The influence of the load trasnfer leads to a change of this moment. The changes per fastener row can be written as:

$$\begin{aligned} \Delta M_1 &= -M_1 + Pe_1 \\ \Delta M_2 &= -M_2 \\ \Delta M_3 &= -M_3 + Pe_3 \end{aligned} \tag{14}$$

These changes in moments must be taken into account when analyzing the deformations in the joint. Note that for the original neutral line model, $T_2 = 0$, $T_1 = T_3 = P/2$ and $e_1 = e_3 = t/2$, it follows that $\Delta M_i = 0$.

The calculation of T_1 and T_2 is based on the different elongations of the upper and lower sheetoccuring as a result of fastener tilting. This phenomenon is described here by a linear function between the applied load (P) transmitted by a row of fasteners and the displacement (δ) occurring in the joint due to plastic deformation around the fastener holes.

$$f = \frac{\delta}{P} \tag{15}$$

For the lap-splice joint, the symbol δ is the displacement of the lower sheet at a row relative to the upper sheet, while P is the load associated with the relevant internal moment (T_1 or T_2). The symbol f is an empirically obtained flexibility constant. For the first and the second row:

$$\begin{aligned} \delta_1 &= f \cdot T_1 \\ \delta_2 &= f \cdot T_2 \end{aligned} \tag{16}$$

The fastener flexibility displacements and the tensile elongations of the upper and lower sheet (ΔL_{upper} and ΔL_{lower}) must be compatible, see Figure 7.

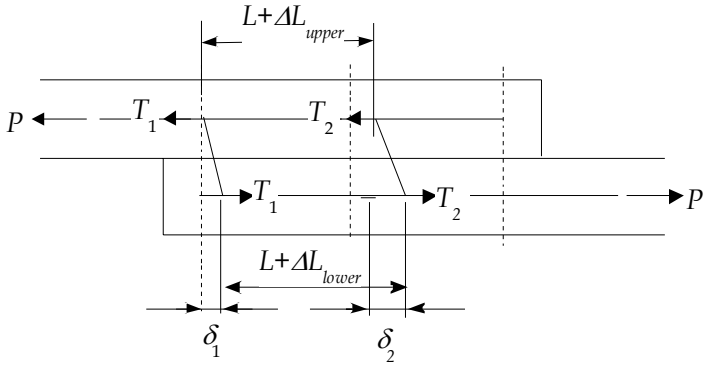

Figure 7 Force distribution when effected by fastener flexibility

The tensile elongations follow from the stress strain relation: $\varepsilon = \frac{\Delta L}{L} = \frac{S}{E} = \frac{load}{AE}$

$$\Delta L = \xi \cdot load \quad \text{with } \xi = \frac{L}{AE} \tag{17}$$

where A is the cross sectional area. For the lap-splice joint in Figure 7 it implies:

$$\begin{aligned} \Delta L_{upper} &= \xi \left(P - T_1\right) \\ \Delta L_{lower} &= \xi \, T_1 \end{aligned} \tag{18}$$

The compatibility between the tensile elongations and fastener flexibility displacements is easily obtained from Figure 7:

$$L + \Delta L_{upper} = \delta_1 + \left(L + \Delta L_{lower}\right) - \delta_2 \tag{19}$$

With L = 28 mm, A = 200 mm^2 and E = 72000 N/mm^2 the ξ-value is:

$$\xi = 1.944 \cdot 10^{-6} \frac{mm}{N}$$

The empirical fastener flexibility according to Huth [7] is:

$$f = 3.523 \cdot 10^{-5} \ \frac{mm}{N}$$

The value of T_1 can now be calculated by substitution of Eqns 16 and 18 in 19, and T_2 follows from Eqn. 11. The results obtained are:

$$T_1 = \left(\frac{\xi + f}{2\xi + 3f} \right) P$$
$$T_2 = \left(\frac{f}{2\xi + 3f} \right) P \qquad (20)$$

With the above-mentioned value of ξ and f the results for T_1 and T_2 are:

$$T_1 = 7052$$
$$T_2 = 5896$$

This load transmission is illustrated by Figure 8. As a result of the fastener flexibility the first fastener row transmits 35 % (7052 N) of the load P, the second row 30 % (5896 N) and the third row again 35 %.

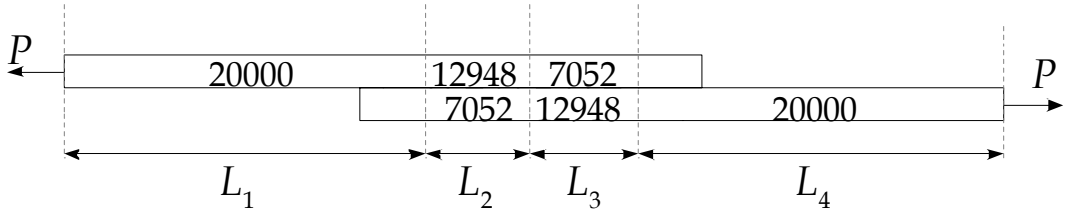

Figure 8 load transfer in the simple lap-splice joint accounting for fastener flexibility

The calculation of the internal moment is entirely dependent on the location of the neutral axis of the lap-splice joint [6]. The internal moment is therefore a function of both the load transfer and the geometric lay-out of the joint. In case of a monolithic joint the neutral line is located at the center of each element of the lap-splice joint. The moments can then be calculated using e_1 = -t/2 and Eqn. 13 and 14:

$$\Delta M_1 = -5896\ Nmm$$
$$\Delta M_2 = 11792\ Nmm$$
$$\Delta M_3 = -5896\ Nmm$$

The bending factor was calculated in the previous Section 2.1 for the simple lap joint without considering rivet tilting. The bending factor will now be derived for the same lap splice joint accounting for rivet tilting and load transmission by all fastener rows.

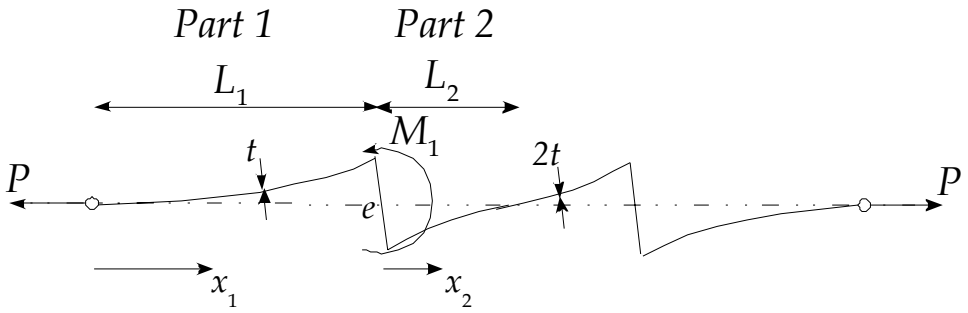

Figure 9 Secondary bending in the simple symmetric lap-splice joint with the internal moments at the first fastener row

For Part 1 in Figure 9 the equations for the bending moment and the displacements $w(x)$ are similar to the Eqn. 1 - 4 with the solution given in Eqn. 5. With the condition that $w(x_1) = 0$ for $x_1 = 0$, it is easily found that $B_1 = 0$. The equation for $w(x_1)$ thus becomes:

$$w(x_1) = A_1 \sinh(\alpha_1 x_1) \tag{21}$$

For Part 2 the internal moment ΔM_1 must be included:

$$M_{x_2} = Pw(x_2) - \Delta M_1 = EI_2 \left(\frac{d^2 w}{dx_2} \right)_{x_2} \tag{22}$$

The solution of this differential equation is:

$$w(x_2) = A_2 \sinh(\alpha_2 x_2) + B_2 \cosh(\alpha_2 x_2) + \frac{\Delta M_1}{P} \tag{23}$$

The boundary conditions at the first fastener row ($x_1 = L_1$ and $x_2 = 0$) are:

$$\left(w_{x_2}\right)_{x_2=L_2} = \left(w_{x_1}\right)_{x_1=L_1} + e_1 \tag{24}$$

$$\left(\frac{dw}{dx} \right)_{x_1=L_1} = \left(\frac{dw}{dx} \right)_{x_2=0} \tag{25}$$

At the end of Part 2 another condition for reasons of symmetry is:

$$(w_2)_{x_2=L_2} = 0 \tag{26}$$

The constants A_1, A_2 and B_2 can now be solved after substitution of Eqns 21 and 23 in Eqns. 24 to 26. With the boundary values of the hyperbolic function written as:

$$S_i = \sinh(\alpha_i L_i)$$
$$C_i = \cosh(\alpha_i L_i)$$
$$Th_i = \tanh(\alpha_i L_i)$$

The three equations are:

$$B_2 = A_1 S_1 - \frac{\Delta M_1}{P} + e_1$$
$$A_2 = \frac{\alpha_1}{\alpha_2} A_1 C_1 \qquad (27)$$
$$A_2 S_2 + B_2 C_2 + \frac{\Delta M_1}{P} = 0$$

The most critical bending moment occurring at the first fastener row is obtained as:

$$M_{x_1=L_1} = EI\left(\frac{d^2 w}{dx^2}\right)_{x_1=L_1} \qquad (28)$$

With $\alpha_1^{\,2} = \frac{P}{EI_1}$ the result for the bending factor becomes:

$$k_b = \frac{\sigma_{bending}}{\sigma_{tension}} = \frac{\frac{6M_c}{Wt^2}}{\frac{P}{Wt}} = \frac{6\alpha_1^{\,2} A_1}{Pt} \qquad (29)$$

After solving A_1 and realizing that $t_2 = 2t$ and $e = -t/2$ for the simple lap-splice joint, a further evaluation leads to:

$$k_b = \frac{\left(\frac{6\Delta M_1}{Pt}\right)\left(1 - \frac{1}{C_2}\right) + 3}{1 + \frac{Th_2}{Th_1} 2\sqrt{2}} \qquad (30)$$

It should be noted that for $\Delta M_1 = 0$, i.e. no fastener flexibility and internal moments, Eqn. 30 reduces to the previous Eqn. 9. Results of the calculations of k_b with fastener flexibility (Eqn. 30) are shown in Table II for similar values of L_1, L_2, t, E used previously.

L_1 [mm]	L_2 [mm]	t [mm]	E [N/mm^2]	f [mm/N]	k_b for an applied stress of 100 MPa	
					With f	Without f
200	28	2	72000	3.542E-5	1.09	1.16
	18				1.39	1.43
	28	1		5.369E-5	0.64	0.88
		2	210000	1.214E-5	1.46	1.49

Table II Variation of input data for symmetrical lap-splice joint, f calculated using Huth [7] this also effects the load transfer through the fastener rows.

The last column of Table 3 includes the results for the same lap joint as calculated in Section 2.1 where tilting of fasteners was not considered. A comparison between the bending factors obtained with and without including fastener flexibility is made in the last two columns of Table II. It turns out that the bending factor is reduced by the fastener flexibility which agrees with expectations about flexibility effects recalled earlier. However, the reduction is relatively small, just a few percent with one exception for t = 1.0 mm (reduction 27%).

The trends of k_b noted in the previous section do not change when the influence of load transfer is taken into account.

- Changing the overlap length from 28 mm to 18 mm still increases the bending factor k_b.
- A decrease in sheet thickness results in a decrease in bending stiffness and thus in a lower k_b.
- Increasing the Modulus of Elasticity for the joint results in a higher bending factor k_b.

In summary:
The fundamental assumption of the present internal moment model is that the load distribution in the two sheets is related to deformations associated with fastener flexibility in order to arrive at compatibility equations from which the load distribution can be calculated. The load distribution then reveals the load transmitted by the fastener rows from which the internal moments can be derived.

In the present section, a calculation was made for the most simple case of a symmetric lap-splice joint to illustrate the basic procedure. Similar calculations can be made with the same model for other joints with a more complex geometry and other materials including fiber metal laminates.

3. RESULTS

In this section results are presented for surface stress levels in two butt splice joints and one in service lap splice joint. Figure 10 shows calculated and measured results of stress levels in an Al-2024 T3 Clad butt splice joint. Only one overlap of the symmetric simple strap joint is shown. The calculations provide a continuous curve of the variation of the stress level along the joint. The strain gage measurements give a number of local stress values only. Outside the overlap the agreement between calculation and measurement is very good. Inside the overlap the agreement is less, but it should be realised that the neutral line model is a one dimensional model which does not take into account the non-homogenous stress distribution in the width direction

Figure 11 shows a similar comparison for a fiber metal laminate butt-splice joint. The trends are practically the same as for the Al-2024 T3 Clad butt splice joint, i.e. again a very good agreement outside the overlap area, and a qualitatively correct trend inside the overlap.

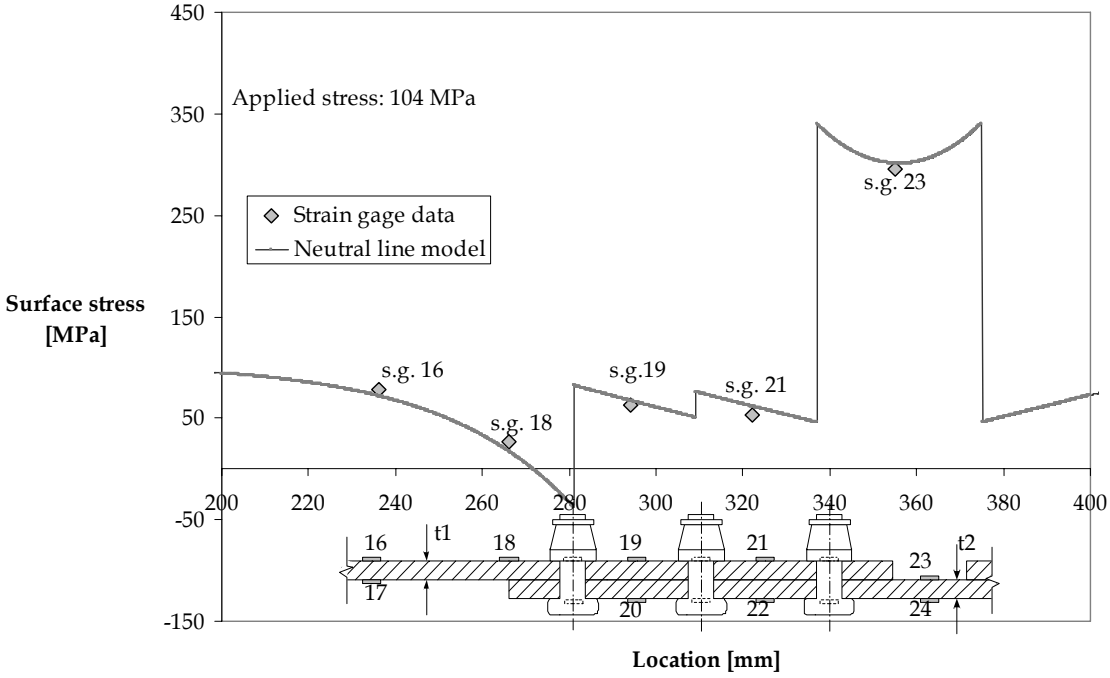

Figure 10 Butt joint results from strain gages at the lower side of the butt splice joint, sheet thickness t_1 = 4.0 mm, t_2 = 4.0 mm and material Al 2024-T3 Clad

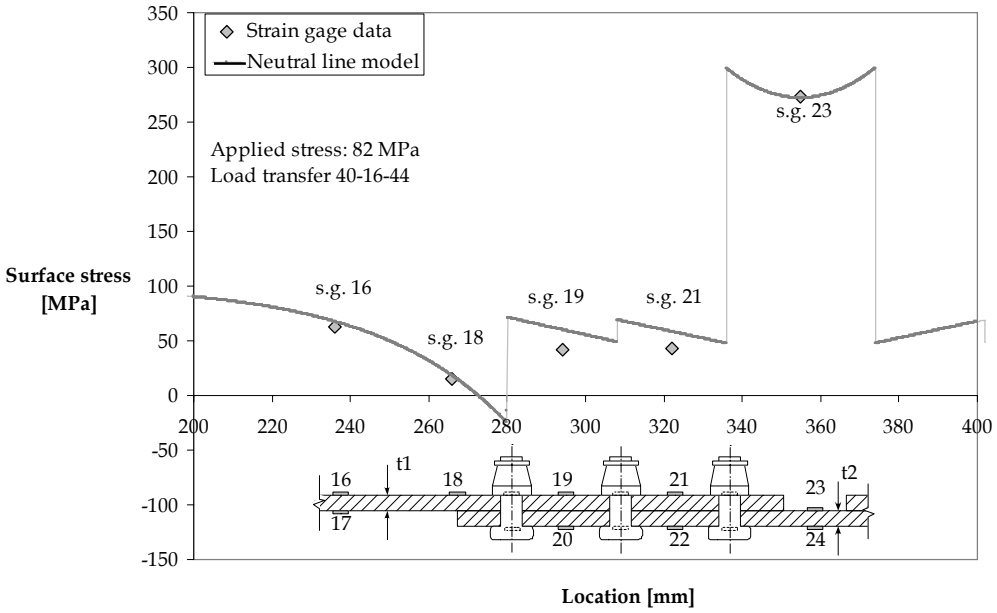

Figure 11 Butt joint surface stress representation for strain gages at the upper surface, sheet thickness t_1 = 4.25 mm, t_2 = 4.25 mm and material sheet 1 is Glare 3-6/5-0.5 and sheet 2 is Glare 2B-6/5-0.5

The results shown in Figure 12 are from a four rivet row lap-splice joint with extra doublers and a longitudinal stiffener attached with only one fastener row. Strain gages for this joint were attached one inch to the right of row *A*. The results for this specimen were obtained by Fawaz [8]. Four different joints were used to obtain strain gage data. With the method described in this paper, the load transfer distribution over the four fastener rows is as follows; 25% load transfer from the skin-material into the doubler. The second fastener row transfers again 25% load from the skin and doubler sheet to the other sheet and doubler. Each fastener row carries 25% of the applied load. As shown for the other joints before, the stresses outside the overlap region are predicted with great accuracy, even for this more complicated joint with doublers.

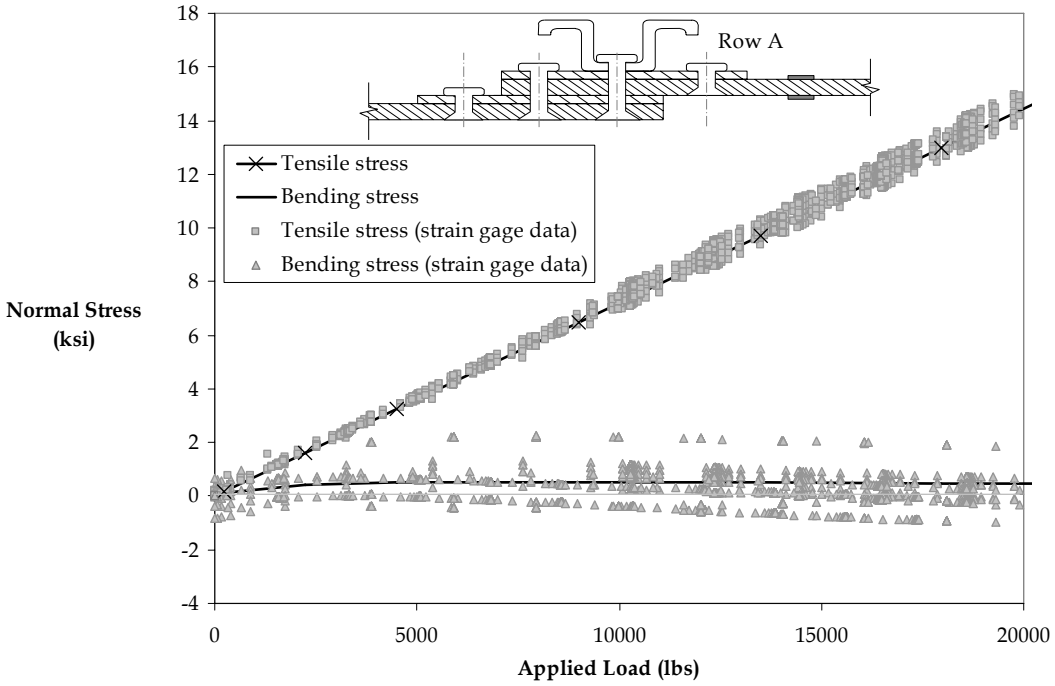

Figure 12 Normal stress one inch to the right of row *A*

4. CONCLUSIONS

1. The internal moment concept gives a good representation of the load transfer occurring in multi-row joints. The calculation of the load transfer can be made for complicated lap-splice and butt joints in both monolithic and laminated sheet materials. The calculated and the experimental stress levels agreed very well outside the overlap area of the joints, while indicative results were obtained in the overlap area. The results provide a base for further research into improved fastener flexibility equations and load transfer.
2. The influence of the fastener flexibility is of less importance than previously expected.
3. Adding doublers and stringers do not offer complications. Only those parts adding bending stiffness to the joint need to be taken into account.

4. The present experience indicates that the neutral line model is a very powerful tool to use in the early stages of joint design. It gives a good picture of critical bending stresses in a joint.

LIST OF SYMBOLS

Latin

A	Area	[mm^2]
A_i, B_i	Constants for solving differential eq.	[mm]
e_i	Eccentricity	[mm]
E	Young's modulus	[MPa]
f	Fastener flexibility	[mm/N]
I	Moment of inertia	[mm^4]
k_b	Bending factor	[-]
L	Length	[mm]
M_i, M_x	Moment	[Nm]
$M_{internal}$	Internal moment	[Nm]
P	Applied force	[kN]
t_i	Thickness	[mm]
T_i	Load transfer	[kN]
w_i	Displacement neutral axis	[mm]
W	Width	[mm]
x	x-coordinate	[mm]
y	y-coordinate	[mm]

Greek

α_i	Stiffness ratio	[MPa]
δ	Displacement	[mm]
$\delta_{f,i}$	Displacement of fastener	[mm]
Δ_i	Displacement of sheet	[mm]
σ_b	Bending stress	[MPa]
$\sigma_{bending}$	Bending stress	[MPa]
$\sigma_{tension}$	Tensile stress	[MPa]
$\xi_{j,i}$	Stiffness ratio	[mm/N]

REFERENCE LIST

[1] Gere, J.M. and Timoshenko, S.P. (1991), *Mechanics of Materials*, Chapman & Hall, London.

[2] Hartman, A. and Schijve, J. (1968), *Effects of dimensions of riveted lap joints and single-strap butt joints on secondary bending (in Dutch)*. NLR-TR-68026, Amsterdam, National Aerospace Laboratory

[3] Schijve, J. (1972), *Some Elementary Calculations on Secondary Bending in Simple Lap Joints*, NLR-TR-72036, Amsterdam, National Aerospace laboratory

[4] Müller, R.P.G. (1995), *An Experimental and Analytical investigation on the Fatigue Behaviour of Fuselage Riveted Lap Joints, The Significance of the Rivet Squeeze Force, and a Comparison of 2024-T3 and Glare 3*, Dis. Delft University of Technology

[5] De Rijck, J.J.M. and Fawaz, S.A. (2001), *A Simplified Approach for Stress Analysis of Mechanically Fastened Joints*, 4th Joint DoD/FAA/NASA Conference on Aging Aircraft

[6] Rijck, J.J.M. (2005), *Stress Analysis of Fatigue Cracks in Mechanically Fastened Joints*, Dis. Delft University of Technology

[7] Huth, H. (1986), In: *ASTM STP 927; Influence of Fastener Flexibility on the Prediction of load transfer and Fatigue Life for Multiple-Row joints*, p. 221-250

[8] Fawaz, S.A. (2000), *Equivalent Initial Flaw Size Testing and Analysis of Transport Aircraft Skin Splices*, In: Fatigue and Fracture of Engineering Materials and Structures, Vol. 26 p. 279-290